


Please cite the Published Version

Shehbaz, Tauheed, Khan, Fahd Nawaz, Junaid, Massab and Haider, Julfikar  (2022) Investigating the bonding mechanism of P-TIG welded CpTi/Inconel 718 dissimilar joint with Nb interlayer. Materials Letters, 313. ISSN 0167-577X

DOI: <https://doi.org/10.1016/j.matlet.2022.131748>

Publisher: Elsevier

Version: Accepted Version

Downloaded from: <https://e-space.mmu.ac.uk/629146/>

Additional Information: This is an Author Accepted Manuscript of an article published in Materials Letters by Elsevier.

Enquiries:

If you have questions about this document, contact openresearch@mmu.ac.uk. Please include the URL of the record in e-space. If you believe that your, or a third party's rights have been compromised through this document please see our Take Down policy (available from <https://www.mmu.ac.uk/library/using-the-library/policies-and-guidelines>)

Investigating the bonding mechanism of P-TIG welded CpTi/Inconel 718 dissimilar joint with Nb interlayer.

Tauheed Shehbaz^a, Fahd Nawaz Khan^a, Massab Junaid^b, Julfikar Haider^c

Abstract

The direct joining of CpTi and Inconel 718 is challenging due to the formation of brittle Ti_xNi_y in the fusion zone. For the TIG welding of CpTi/IN718 joints in the present work, the use of Nb as an interlayer served as a barrier, resulting in the complete suppression of brittle Ti_xNi_y which is responsible for immediate failure of the CpTi/IN718 dissimilar joint. The results indicated that solid solution formed towards the CpTi side, whereas eutectic formation ($NbNi_3$, Nb_7Ni_6) was observed towards the IN718 side of the weldment. Owing to these brittle IMCs, a nanohardness of ~ 14.62 GPa was measured at the Nb/IN718, which is ~ 70 % higher than that of the Nb/CpTi interface which was comprised of columnar dendrites. The tensile strength was 150 MPa with the presence of cleavage cracks at the Nb /IN718 interface of the fractured surface.

Key words: Welding, CpTi, Inconel 718, nanoindentation, microstructures

1. Introduction:

Ni-based superalloys possess unique mechanical properties at high temperatures due to the presence of strengthening elements such as Cr, Fe and Nb and are widely used in manufacturing of gas turbine components, rocket and aircraft engine [1,2]. Commercially pure titanium's (CpTi) exceptional biocompatibility, high specific strength, and corrosion resistance make it an attractive choice for applications in the biomedical engineering, aerospace and automobile industries [3,4]. However, the direct joining of Ti and Ni alloys is highly challenging due to the formation of brittle IMCs, cracks, and residual stresses in the weldments [5]. Some of the proposed solutions to prevent the formation of IMCs is by modifying the chemical composition of the weld zone and increasing the solidification rate[6]. Interlayer is one of the methods to inhibit the formation of IMCs. Niobium (Nb), with a high melting point (2468°C) and

1
2
3
4 excellent thermophysical characteristics, has proved to be a successful interlayer due to its high
5
6 compatibility and strengthening effect on Ti alloys. Furthermore, the Ti, Nb binary phase diagram indicates
7
8 the formation of solid solution of Ti with Nb in every proportion. The current study seeks the use of Nb as
9
10 an interlayer on microstructures and the interfacial strength of dissimilar CpTi /IN718 TIG weldment.
11
12

13 **2. Experimental Method**

14
15 The weldments were produced using $80 \times 50 \times 1 \text{ mm}^3$ sheets of CpTi (Ti: Base, Fe: 0.15, C: 0.04, O: 0.15 in
16
17 at. % and IN718 (Ni: Base, Fe: 18.61, Cr: 21.75, Nb: 5.29, Mo: 1.61, Ti: 1.02, Co: 0.09, Al: 0.88 in at. %) . The
18
19 TIG welding process was carried out and important welding parameters were identified for full
20
21 penetration in the alloy sheets and partial melting of Nb interlayer through initial trials. The optimized
22
23 parameters were current: 91A, Arc voltage: 11V, welding speed: 400 mm/min, Arc length: 3mm and gas
24
25 flow rate: 15 L/min.
26
27
28

29
30 The etching solutions employed for the IN718 and CpTi were $2\text{g CuCl}_2 + 15 \text{ ml HCl} + 5 \text{ ml HNO}_3 + 5 \text{ ml H}_2\text{O}$
31
32 and Kroll solution (2% HF in distilled water), respectively. The etched samples were characterized using a
33
34 polarizing microscope, XRD and SEM equipped with an (EDS). Specimens for tensile testing were
35
36 produced, following the ASTM standard E8M-04 [7] with interlayer in the centre of the gauge length, using
37
38 an Instron machine at a strain rate of 1 mm/min. Nanoindentation was performed at a constant load of
39
40 200 mN.
41
42
43

44 **3. Results and Discussions**

45
46 In **Figure 1**, the relatively large width of the fusion zone on the CpTi side in the CpTi/IN718 weldment can
47
48 be attributed to the high specific heat of the CpTi (520 J/Kg-K) as compared to the IN718 (430 J/Kg-K)
49
50 causing absorption of majority of the heat rather than dissipating to the bulk alloys [8]. Zone A in **Figure**
51
52 **1(b)** shows equiaxed α grains of the Ti base metal (BM) with β grains at the grain boundaries. Zone B
53
54 comprises of relatively planar grains, which grew epitaxially from the base metal as shown in **Figure 1(c)**.
55
56 This may be due to the partially melted base metal surface, functioning as a nucleating surface for the
57
58
59
60
61
62
63
64
65

molten weld and leads to the competitive grain growth process. FZ (zone C) and melt zone (zone D) can be seen in **Figure 1(d)** and **Figure 1(e)**, respectively. The microstructural difference in the two zones may be attributed to the low heat input due to the high welding speed and thermal conductivity of the CpTi fast cooling rate, resulting in a sharp thermal gradient in the weldments. The FZ on the IN718 side shown in **Figure 1(f)**, comprise of cellular and columnar dendrites. Furthermore, a thin white diffused layer at the Nb/IN718 interface can be seen, which might be due to the interdiffusion of Nb and Ni. Further dissolution of the Nb interlayer in the adjacent alloys is evident from the variation in width of the Nb interlayer as shown in **Figure 1(a)**.

Figure 2(a) presents a cross-section of the welded joint with the Nb interlayer. The MZ in **Figure 2(b)**, comprises of columnar dendrites. The EDS results in **Table 1**, indicate the Ti and Nb as the major elements, suggesting absence of IMCs. However, the presence of Ni, Cr and Fe in this region can be associated with the dissolution of IN718 in CpTi due to the melting of the arc facing side. Moreover, the interface shown in **Figure 2(c)** contains 96.28% Ti and 3.72% Nb, indicating the formation of solid solution. Owing to the high wettability and convection currents, a defect free CPTI/Nb interface is formed as shown in **Figure 2(d)**. Moreover due to complete solubility[9], the (Ti, Nb) solid solution was formed. The line scans (L1 and L2) in **Figure 2** show the dissolution of Nb in Ti at CpTi side, which can be attributed to the convection currents and Marangoni effect [10]. The difference in the chemical composition, high heating, and cooling rates of the TIG welding process, prevented the intermixing of Ti and Nb in the FZ [11] and resulted in less diffusion of Nb in Ni along L2.

Table 1: EDS (at. %) analysis of the MZ and at the interface of the CpTi side.

Spot	Ti	Cr	Fe	Ni	Nb
i	47.01	8.31	7.25	15.9	21.53
ii	25.63	8.94	2.90	2.68	58.02
iii	96.28	3.72	-	-	-

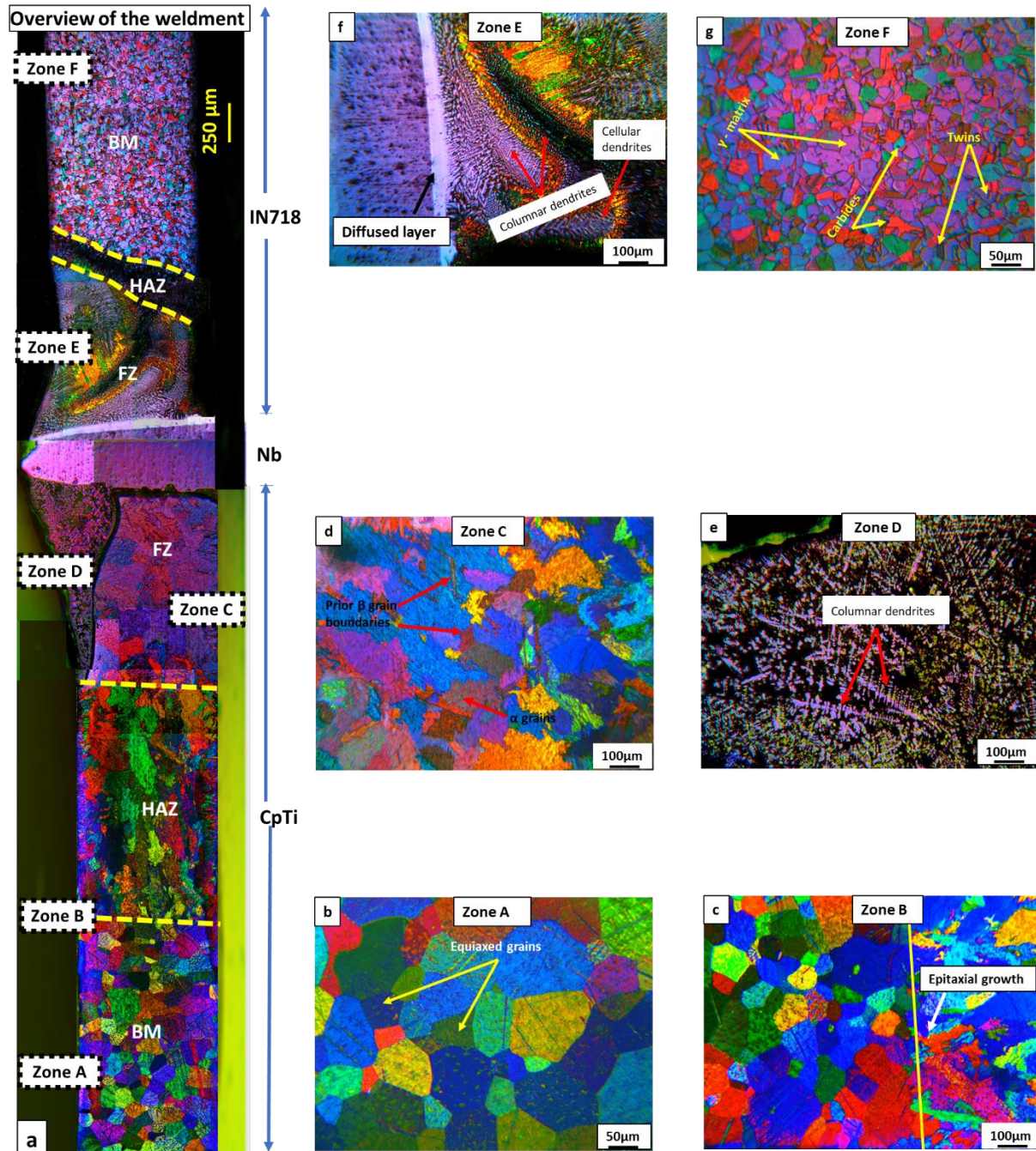
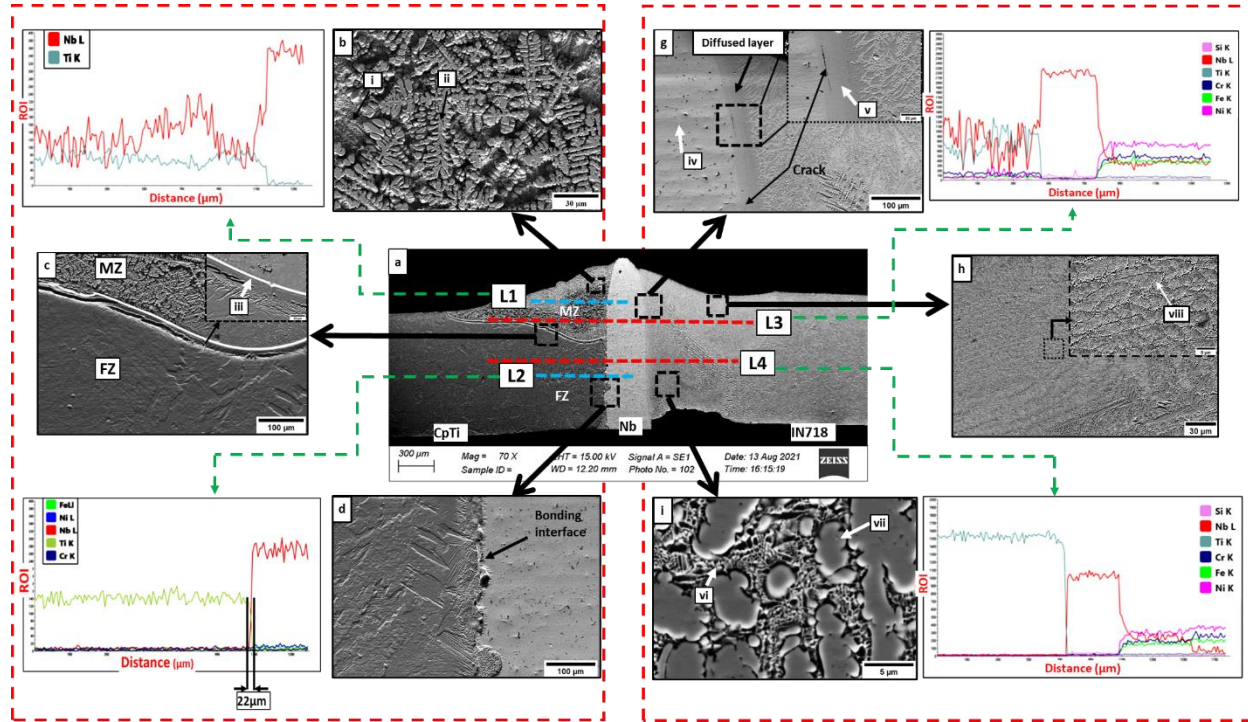


Figure 1: Microstructure of the weldment.

The diffused layer at the IN718 and Nb interface can be seen in **Figure 2 (g)**, which varied from ~ 35 to 57 μm at the arc facing to the bottom side of the weldment. This is owing to the higher dissolution of the Nb in Ni. According to EDS results, the diffused layer is composed of Ni_3Nb . In **Figure 2(i)**, the majority of the region comprises of eutectic mixture and γ -matrix as can be seen in **Figure 2(h)**. The potential phases in

1
2
3
4 this region are listed in **Figure 2**. The formation of the eutectic mixture can be attributed to the
5
6 spontaneous melting which occurred at the IN718 and Nb interface when the temperature exceeded
7
8 1170°C. During the TIG welding and rapid solidification, the Ni_3Nb IMC nucleated first during cooling,
9
10 resulting in a higher concentration of the Nb in the liquid, leading to a eutectic reaction. Furthermore, the
11
12 region shown in **Figure 2(h)**, is entirely composed of lamellar eutectic microstructure.
13
14
15



Position	Ni	Nb	Cr	Fe	Mo	Ti	Possible Phases
iv	-	100	-	-	-	-	Nb
v	34.33	38.48	12.87	12.82	1.51	-	$NbNi_3$, Nb_7Ni_6
vi	38.74	26.99	15.98	12.14	2.84	3.32	Nb_7Ni_6 , $NbNi_3$
vii	50.2	5.93	18.14	19.11	3.17	3.45	$Ni(\gamma)$
viii	48.31	8.37	18.6	18.22	4.18	2.32	Ni , $NbNi_3$

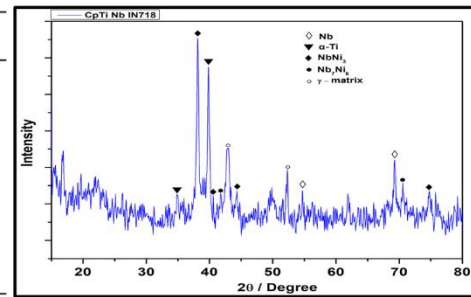


Figure 2: (a) SEM, line scans and XRD of welded joint.

53
54
55 EDS line scan along L3 and L4 shows no diffusion of Ni and Ti across the interlayer. The presence of
56
57 numerous cracks in **Figure 2(g)** can be related to the temperature field distribution, shrinkage strains,
58
59 residual stresses, and the brittle nature of IMCs [12]. XRD: The XRD spectra of in **Figure 2**, shows the
60
61
62
63
64
65

presence of two IMCs, $NbNi_3$ and Nb_7Ni_6 . The (p - h) curves of the Nb/CpTi interface and neighboring regions are presented in **Figure 3(c)**. On Nb/CpTi side, the MZ depicting ~ 1500 nm penetration depth which increased to a maximum of ~ 3100 nm in the Nb interlayer. However, on the Nb/IN718 side, in **Figure 3(d)**, the diffused layer showed 194% and 78% higher resistance to indentation than interlayer and BM, indicating high brittleness. The presented data in **Figures 3(e)** and **3(f)** show a maximum hardness of ~ 7 GPa in MZ zone of the CpTi side can be associated with the dissolution of Nb and Ti resulted a solid solution. The nanohardness of the FZ is relatively less than the BM in **Figure 3(e)** and in good agreement with the microstructures of both regions. Similarly, the maximum nanohardness of ~ 14.62 GPa at the diffused layer is ~ 10.3 and ~ 3.7 times higher than the interlayer and the BM of IN718 alloy, respectively.

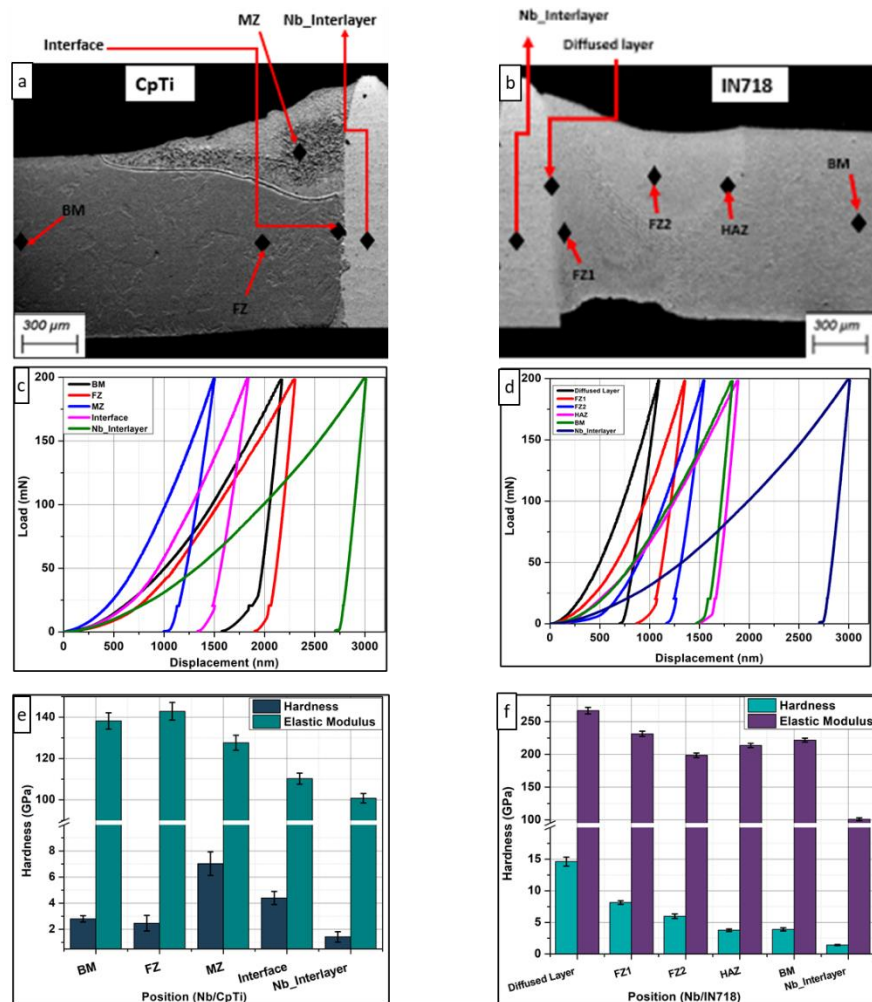


Figure 3: Nanoindentation of the weldment.

Overall strength of the CpTi/Nb/IN718 weldment (150 MPa) is less than both the base alloys, CpTi (360 MPa) and IN718 (850 MPa) respectively. The reduction in the UTS of the weldment could be attributed to the existence of cracks, brittle IMCs, and development of residual stresses during the welding. **Figure 4** presents the fractured surface of the joint and its EDS analysis. The fractured surface had a cleavage appearance, indicating brittle fracture. EDS analysis at (a) and (b) indicated the Ni-Nb IMCs, which suggested that the joint failure took place at the Nb/IN718 interface.

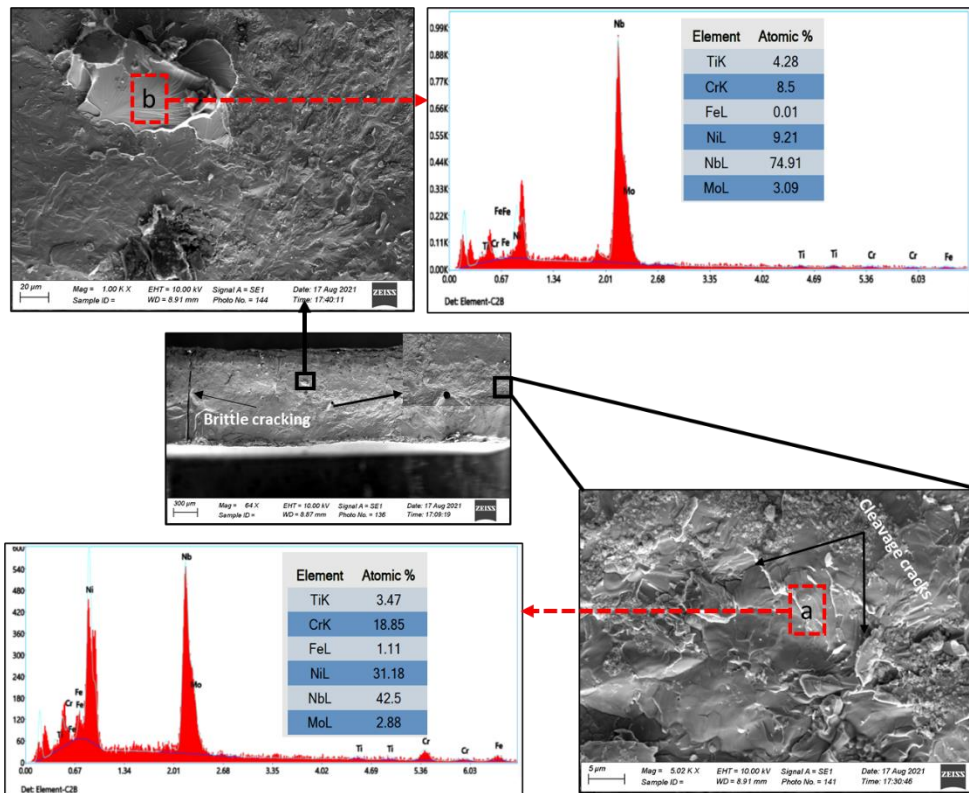


Figure 4: Fractured surface of the CpTi/Nb/IN718 joint.

3. Conclusions:

After successful production and characterization of the welded joint, the following conclusions were drawn:

- The melted region at the arc facing side of the CpTi showed dissolution of Nb in higher proportion due to the high temperature of arc and thermal conductivity of the CpTi.

- 1
2
3
4
5
6
7
8
9
10
11
12
13
14
15
16
17
18
19
20
- Nb acted as an efficient barrier to the formation of the brittle Ni/Ti IMCs. The low strength (150 MPa) can be associated to the existence of cracks, high residual stresses, and brittle IMCs.
 - The CpTi and Nb interface had a columnar dendritic structure which is evident of the formation of solid solution whereas the Nb/IN718 interface displayed the eutectic reaction, resulting in the formation of NbNi₃, Nb₇Ni₆ intermetallics.
 - The diffused layer showed the maximum nanohardness (~ 14.62 GPa), which was ~ 10.3 and ~ 3.7 times higher than the Nb interlayer and the BM of the IN718 alloy, respectively.

21
22

References

- 23
24
25
26
27
28
29
30
31
32
33
34
35
36
37
38
39
40
41
42
43
44
45
46
47
48
49
50
51
52
53
54
55
56
57
58
59
60
61
1. D. Zhang, Z. Feng, C. Wang, W. Wang, Z. Liu, and W. Niu, *Mater. Sci. Eng. A* **724**, 357 (2018).
 2. O. Dziuba, G. Cempura, A. Wusatowska-Sarnek, and A. Kruk, *J. Mater. Eng. Perform.* **29**, 1515 (2020).
 3. M. Zhu, G. Wu, Y. Li, and X. Huang, *Cailiao Daobao/Materials Rev.* **32**, (2018).
 4. B. Wysocki, P. Maj, A. Krawczyńska, K. Roźniatowski, J. Zdunek, K. J. Kurzydłowski, and W. Świążkowski, *J. Mater. Process. Technol.* **241**, 13 (2017).
 5. S. Chatterjee, T. A. Abinandanan, G. M. Reddy, and K. Chattopadhyay, *Metall. Mater. Trans. A Phys. Metall. Mater. Sci.* **47**, 769 (2016).
 6. A. Shojaei Zoeram and S. A. A. Akbari Mousavi, *Mater. Lett.* **133**, 5 (2014).
 7. ASTM E8, *Annu. B. ASTM Stand.* 4 1 (2010).
 8. J. Valencia and P. Queded, (2013).
 9. V. Fallah, M. Amoozraei, N. Provas, S. F. Corbin, and A. Khajepour, *Acta Mater.* **60**, 1633 (2012).
 10. K. C. Mills, B. J. Keene, R. F. Brooks, and A. Shirali, *Philos. Trans. R. Soc. A Math. Phys. Eng. Sci.* **356**, 911 (1998).
 11. J. P. Oliveira, B. Panton, Z. Zeng, C. M. Andrei, Y. Zhou, R. M. Miranda, and F. M. B. Fernandes, *Acta Mater.* **105**, 9 (2016).

1
2
3
4
5
6
7
8
9
10
11
12
13
14
15
16
17
18
19
20
21
22
23
24
25
26
27
28
29
30
31
32
33
34
35
36
37
38
39
40
41
42
43
44
45
46
47
48
49
50
51
52
53
54
55
56
57
58
59
60
61
62
63
64
65

12. Z. Wang, J. Shen, S. Hu, T. Wang, and X. Bu, J. Manuf. Process. **60**, 54 (2020).